Water Research 218 (2022) 118476

Contents lists available at ScienceDirect

Water Research

journal homepage: www.elsevier.com/locate/watres

Towards realistic predictions of microplastic fiber transport in aquatic environments: Secondary motions

Clarence Edward Choi, Jiaqi Zhang *, Zhengyu Liang

The Department of Civil Engineering, The University of Hong Kong, HKSAR, China

ARTICLE INFO

Keywords:
Microplastic fiber transport
Aquatic environments
Secondary motions
Settling orientation
Orientation-dependent drag model

ABSTRACT

Microplastics fibers are abundant in aquatic environments and are an emerging environmental threat. Understanding how fibers are transported in aquatic environments is essential for identifying pollution hotspots and developing remediation strategies. Over recent years, an increasing number of drag models have been proposed to describe the transport of microplastics in aquatic environments. However, none of the proposed models consider secondary motions, which are responsible for non-vertical settling motions. To investigate the role of secondary motions, an experimental setup with an image processing technique was developed to capture the spatial-temporal kinematics of microplastic fibers settling in quiescent water. A new drag model, which adopts the crosswise sphericity to consider the effects of secondary motions of a microplastic fiber and the Aschenbrenner shape factor to account for the unique morphology of the microplastic fiber, was proposed and evaluated. Secondary motions of microplastic fibers have profound effects on their settling trajectories and deposited positions. The settling motion and drag coefficient of a microplastic fiber is an orientation-dependent process. Moreover, the secondary motion is strongly dependent on the fiber dimension and density. The here-proposed drag model is proven to more accurately characterize the settling motion of microplastic fibers compared to existing models that neglect secondary motions. The methodology and model from this study can be used to progress towards improved and realistic predictions of the transport of microplastic fibers in aquatic environments.

1. Introduction

Microplastic pollution has emerged as a pressing environmental concern (Blettler et al., 2018). In particular, aquatic environments are a major sink for microplastic pollution (Zhao et al., 2019). Among the microplastics detected in aquatic environments, fibers, which are generally released from laundry effluent (Napper and Thompson, 2016) and fishing gear (Xue et al., 2020), are commonly reported (Chen et al., 2021). More importantly, microplastic fibers have been traced in the food chain (Bessa et al., 2018), which may pose a threat to human health (Senathirajah et al., 2021). Evidently, the identification of pollution hotspots and remediation strategies are urgently needed. To tackle this problem, the improved prediction of the transport of microplastic fibers is a prerequisite (Zobkov et al., 2019). This is because transport governs the concentration depth profile (Cowger et al., 2021) and residence time (Khatmullina and Isachenko, 2017) of microplastic fibers in aquatic environments.

Generally, the transport of microplastics in aquatic environments can be modeled using the modified Maxey-Riley equation (DiBenedetto et al., 2018; Roy et al., 2022), which is expressed as follows (Yin et al., 2003):

$$m_m \frac{du_m}{dt} = F_G + F_B + F_D + F_L + F_V + F_P \tag{1}$$

where m_m is the microplastic mass, $\boldsymbol{u_m}$ is the microplastic velocity, t is the motion time of the microplastic, and d/dt is the time derivative following the moving microplastic. The terms on the right side of Eq. (1) represent the forces due to gravity ($\boldsymbol{F_G}$), buoyancy ($\boldsymbol{F_B}$), drag ($\boldsymbol{F_D}$), lift ($\boldsymbol{F_L}$), virtual mass ($\boldsymbol{F_v}$), and pressure gradient in the fluid ($\boldsymbol{F_P}$), respectively. In industrial processing, the Basset history force and Faxén terms are generally neglected where particles are considered to be large. For example, Yin et al. (2003) and Carranza and Zhang (2017) ignored these two terms for particles with lengths of 50 mm and 20.2 mm, respectively. As such, the Basset history force and Faxén terms are generally neglected for microplastic particles (DiBenedetto et al., 2018; Roy et al.,

* Corresponding author.
E-mail address: jiaqizjq@hku.hk (J. Zhang).

https://doi.org/10.1016/j.watres.2022.118476
Received 10 January 2022; Received in revised form 1 April 2022; Accepted 15 April 2022
Available online 19 April 2022

2022). Eq. (1) can be expanded to show each force as follows (Yin et al., 2003):

$$m_m\frac{d\boldsymbol{u_m}}{dt} = m_m g - m_m\frac{\rho_f}{\rho_m}g + \frac{1}{2}C_D\rho_f A_P\left(\boldsymbol{u_p}-\boldsymbol{u_f}\right)^2 + \frac{1}{2}C_L\rho_f A_P\left(\boldsymbol{u_p}-\boldsymbol{u_f}\right)^2$$

$$+\frac{1}{2}m_m\frac{\rho_f}{\rho_m}\frac{d}{dt}\left(\boldsymbol{u_p}-\boldsymbol{u_f}\right) + \rho_f\frac{m_m}{\rho_m}\frac{D\boldsymbol{u_f}}{Dt} \quad (2)$$

where ρ_m and ρ_f are the particle and fluid densities, respectively, g is the gravitational acceleration, $\boldsymbol{u_f}$ is the fluid velocity, C_D and C_L are the drag and lift coefficients, respectively, A_p is the projected area of the particle normal to the settling direction, and D/Dt is the time derivative of the fluid element.

When using Eq. (2) to model the transport of microplastic fibers in aquatic environments, the physical properties of the microplastic fiber and fluid (i.e., m_p, ρ_p, ρ_f, *and* A_p) can be measured and the kinematics of the microplastic fiber and fluid (i.e., $\boldsymbol{u_p}$ and $\boldsymbol{u_f}$) are obtained by using the time derivative of the displacement at each time step. For a cylindrical particle (e.g., microplastic fiber), Mando and Rosendahl (2010) reported that its drag coefficient governs its settling motion and its lift coefficient governs its lateral motion. The lift coefficient of a cylindrical particle can be estimated using its drag coefficient and settling orientation (Yin et al., 2003; Zastawny et al., 2012) as follows:

$$C_L = C_D \cdot cos^2\theta \cdot sin\theta \quad (3)$$

where θ is the settling orientation, which is defined as the angle between the principal axis of the particle and the horizontal plane. Evidently, appropriate drag coefficients are central to obtaining reasonable predictions of both the settling and lateral motions of microplastic fibers in aquatic environments.

While a multitude of drag models have been proposed for the prediction of the drag coefficients of microplastic fibers settling in water (Khatmullina and Isachenko, 2017; Waldschlager and Schuttrumpf, 2019; Zhang and Choi, 2022), existing models do not take into account the effects of the secondary motions on the drag coefficients. In fact, it has been demonstrated in other disciplines that secondary motions strongly influence the drag coefficient (Chow and Adams, 2011; Will et al., 2021). This is because secondary motions, which are the oscillatory behaviors of a particle as it settles in quiescent water, are generally initiated by shedding wake vortices (Bagheri and Bonadonna, 2016). With secondary motions, the pressure acting along the surface of the particle is redistributed (Chow and Adams, 2011), which causes an additional lift force to change the settling orientation (Zastawny et al., 2012). Both the lift force and settling orientation induced by secondary motions can affect the drag coefficient, and thus, the transport of microplastic fibers (cf. Eq. (3)).

To characterize the effects of secondary motions on the drag coefficient, Holzer and Sommerfeld (2008) and Song et al. (2017) adopted the crosswise sphericity (i.e., the ratio of the projected area of the volume equivalent sphere of the particle to the projected area of the particle normal to the settling direction) in their drag models. However, the applicability of the models proposed by Holzer and Sommerfeld (2008) and Song et al. (2017) for predictions of the drag coefficients of microplastic fibers remains questionable. This is because Holzer and Sommerfeld (2008) and Song et al. (2017) proposed their drag models for non-microplastic particles in industrial processing (e.g., aluminum and steel particles) and adopted sphericity (i.e., the ratio of the surface area of the volume equivalent sphere of the particle to the surface area of the particle normal to the settling direction) as a second shape factor, which has been demonstrated to have limitations for describing the morphology of microplastic fibers (Zhang and Choi, 2022). Thus, a drag model that can characterize the secondary motions of microplastic fibers is required to improve predictions of their transport in aquatic environments. The aforementioned drag models in the literature for microplastic fibers and non-microplastic particles are summarized in Table S1 of the Supplementary Material.

This study aims to reveal and characterize the effects of the secondary motions of microplastic fibers on their transport. To achieve this, an experimental setup is developed along with a novel image processing technique to capture the secondary motions of the settling microplastic fibers. A new drag model is developed to consider the effects of secondary motions. The experimental data is then used to evaluate the newly-developed drag model.

2. Materials and methods

2.1. Microplastic fibers

The microplastic fibers used in this study were cut from strands of polyester ropes. The titration method (Section SM2 of the Supplementary Material) was used to measure the density of the microplastic fibers (ρ_m=1308 kg/m^3). The length and diameter of each microplastic fiber were measured based on images captured by the digital microscope (Section SM3 of the Supplementary Material). The microplastic fiber lengths range from 5 to 15 mm, and the fiber diameters range from 0.45 to 0.85 mm, which are dimensions that are commonly used in similar settling experiments (Waldschlager and Schuttrumpf, 2019).

2.2. Experimental setup

The experimental setup consists of a water column, image acquisition system, and illumination system (Fig. 1a).

The settling motion of a given microplastic fiber in the water column is tracked by using a camera that captures videos with images at a pixel resolution of 1920 × 1080 and a frame rate of 50 frames per second. A mirror was placed at the side of the column to enable the reflection of the motion of a given microplastic fiber from the side of the column. By adjusting the position of the camera, the camera can be used to simultaneously capture the motion of a given microplastic fiber from both its front and reflected side view in the mirror. Fig. 1b shows a pair of images captured from two different views. A given microplastic fiber will have the same vertical coordinate (i.e., y and y' coordinates in Fig. 1b) in the front and reflected side views, which can later be used as a frame of reference to reconstruct its 3D setting motion. The advantage of this setup is that it enables images from two different views (i.e., front and reflected side) to be captured without the need for multiple cameras (cf. Will et al., 2021).

To ensure high-quality images, an illumination system is required. The system consists of LED lamps with diffusers. The experimental setup was placed inside a darkroom to avoid the influence of external lighting. A white backdrop was positioned behind the column to maximize the color contrast between a given fiber and its background.

2.3. 3D reconstruction of microplastic fiber kinematics

Obtaining the kinematics of a microplastic fiber (e.g., settling velocity and settling orientation) is a prerequisite for capturing its secondary motion. Generally, the settling velocity of a microplastic fiber can be determined by using either the particle tracking velocimetry (PTV) technique (Nguyen et al., 2020) or particle image velocimetry (PIV) technique (Waldschlager and Schuttrumpf, 2019). Both PTV and PIV can be used to track the velocity of an object by dividing the displacement between two successive frames by the time interval (Qureshi et al., 2020). The main difference between PTV and PIV lies in how the particle displacement is obtained. More specifically, PTV tracks the motion of an individual particle, whereas PIV tracks the image texture to acquire the particle displacement (Gollin et al., 2017). However, both PTV and PIV techniques regard a given microplastic fiber as a point mass and thus cannot be used to determine its settling orientation, which needs to be calculated by using the 3D coordinates of its endpoints (Carranza and Zhang, 2017). To address this problem, an image

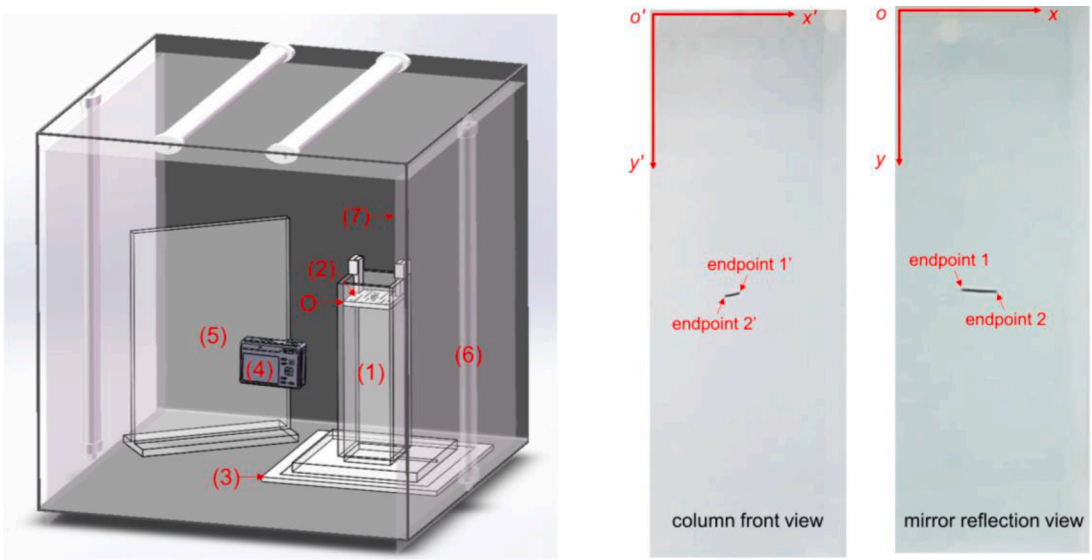

(a) (b)

Fig. 1. Experimental setup for studying secondary motions of microplastic fibers settling in water. (a) Schematic of the experimental setup. The main individual components of the setup are annotated as: 1) water column; 2) fiber release platform; 3) base LED lamp; 4) SLR camera; 5) mirror; 6) side LED lamp; 7) diffuser; O: the origin of the coordinate system adopted for fiber tracking; and (b) Pair of typical captured images from the front of the water column and the mirror reflection view of the same fiber. The length and diameter of the fiber shown are 15 mm and 0.65 mm, respectively.

processing method was developed to identify the endpoints of a settling microplastic fiber in real-time. Details of the image processing method are provided in Section SM4 of the Supplementary Material. Herein we only briefly introduce the development of the image processing method and how it reconstructs the 3D kinematics of a microplastic fiber settling in water.

Since only a single camera is used to synchronously capture the two planes of interest, the captured microplastic fiber contours will inevitably be distorted (Wu et al., 2019). To address this problem, the perspective transformation algorithm is adopted. After which, each corrected image is converted into binary using the background subtraction technique (Piccardi, 2004). After binarization, a given microplastic fiber contour on each image appears as a white area against a black background. The endpoints of a given microplastic fiber from each pair of binarized images can then be identified using the Moore-Neighbor Tracing algorithm embedded in MATLAB. The last step is to reconstruct the settling motion of a given microplastic fiber in three dimensions based on the 2D coordinates of its endpoints. Since the pair of images share the same vertical edge (Fig. 1b), the 3D coordinate of each endpoint can be found by comparing the vertical coordinates of a pair of images (i.e., y and y' coordinates in Fig. 1b). Subsequently, an iterative procedure can be used to process each pair of images to record the time history of the 3D coordinates of each endpoint of a given microplastic fiber. With the time-varying 3D coordinates, the spatial-temporal kinematics of a given microplastic fiber that is settling, including its position, velocity, and orientation in the 3D space can be obtained (Section SM5 of the Supplementary Material).

To evaluate the reliability of the proposed image processing method, we compare reconstructed settling orientations and velocities against the ones measured from the experiments. The evaluation details are provided in Section SM6 of the Supplementary Material. The evaluation results show that the proposed image processing method can successfully track the 3D motions of a given settling microplastic fiber.

2.4. Characterization of settling hydrodynamics of microplastic fibers

Based on Eqs. (1) and (2), the settling motion of a microplastic fiber in quiescent water can be expressed as follows:

$$\rho_m V_m \frac{du_z}{dt} = \rho_m V_m g - \rho_f V_m g - \frac{1}{2} C_D \rho_f A_P u_z^2 - \frac{1}{2} \rho_f V_m \frac{du_z}{dt} \tag{4}$$

where V_m is the microplastic fiber volume that is determined based on the fiber mass (M) and density (ρ_m) or estimated by using the fiber length (L) and diameter (D), i.e., $V_m = M/\rho_m \approx 0.5\pi L D^2$, and u_z is the settling velocity of the microplastic fiber. It should be noted that the force due to the pressure gradient in the fluid (i.e., the last term in Eq. (2)) is neglected herein because one-way coupling between the settling microplastic fiber and water is assumed. More specifically, the settling microplastic fiber is assumed not to influence its ambient fluid field (DiBenedetto et al., 2018; Roy et al., 2022). With this assumption, the fluid velocity ($\boldsymbol{u}_f$) is zero, and thus the force due to the pressure gradient is zero (cf. Eq. (2)).

The projected area of a given microplastic fiber settling with its principal axis parallel to the horizontal plane is calculated as the product of its length and diameter, i.e., $A_P = LD$. If a microplastic fiber settles at an orientation with an angle (θ) between its principal axis and the horizontal plane, then its projected area is calculated as $A_{P,\theta} = A_P \cos\theta$. Thus, combining $A_{P,\theta}$ with Eq. (4), the drag coefficient can be expressed as follows:

$$C_{D,\theta} = \frac{1}{\cos\theta} \frac{2V_m}{A_P u_z^2} \left[\left(\frac{\rho_m}{\rho_f} - 1 \right) g - \left(\frac{1}{2} + \frac{\rho_m}{\rho_f} \right) \frac{du_z}{dt} \right] \tag{5}$$

Based on Eq. (5), an orientation-dependent drag coefficient ($C_{D,\theta}$) can be obtained by using the settling velocities and orientations measured from the experiments of this study.

2.5. Experimental program and procedures

The lengths of the microplastic fibers tested in this study were varied as 5 mm, 10 mm, and 15 mm, respectively. The diameters of these microplastic fibers are 0.45 mm, 0.55 mm, 0.65 mm, and 0.85 mm, respectively. To ensure repeatability, each test was conducted three times for a total of 36 unique tests. The details of the test program are provided in Table S2. After each experiment, the images captured were processed by using the proposed 3D reconstruction method. Then, the

kinematics and hydrodynamics of each settling microplastic fiber were interpreted. The detailed test procedures are described in Section SM7 of the Supplementary Material.

3. Results

3.1. Settling velocity

The temporal change in the settling velocity of a typical microplastic fiber (test ID: L05D45) is shown (Fig. 2). The microplastic fiber initially accelerates (i.e., acceleration stage) before reaching a steady velocity (i.e., steady stage). Despite exhibiting some velocity fluctuations during the steady stage, the relative errors (*RE*) between the maximum (i.e., u_{z1max}, u_{z2max}, u_{z3max}) and minimum (i.e., u_{z1min}, u_{z2min}, u_{z3min}) velocities are smaller than 5 %. Thus, the average values of the measured velocities in the steady stage (i.e., u_{zt1}, u_{zt2}, u_{zt3}) can be considered as the steady settling velocities of the microplastic fibers (Waldschlager and Schuttrumpf, 2019). The maximum relative error (RE_{max}) of the steady settling velocities among the three repeated tests is 4.3%, which indicates a high degree of repeatability. The time history of the settling velocities of all microplastic fibers used in this study is provided in Section SM8 of the Supplementary Material. All microplastic fibers tested in this study reach their steady settling velocities after an acceleration stage.

3.2. Settling trajectory and deposited position

Fig. 3a shows the reconstructed 3D settling trajectories of three typical microplastic fibers used in this study (test IDs: L05D85, L10D65, and L15D55). It can be observed that the microplastic fibers, which were all dropped from the centroid of the releasing platform (cf. Fig. S9a), do not settle vertically in the column. Also, the microplastic fibers are observed to settle at different orientations in the 3D space. The reconstructed 3D settling trajectory of all microplastic fibers tested in this study is provided in Section SM9 of the Supplementary Material.

The observed non-vertical settling trajectories and settling orientations demonstrate the importance ofsecondary motions. Moreover, the final deposited position of the microplastic fibers tested in this study is perhaps one of the most telling indicators of non-vertical trajectories (Mrokowska, 2018). The final positions follow a normal distribution around the position at the onset of the settling motion (Fig. 3b). Findings

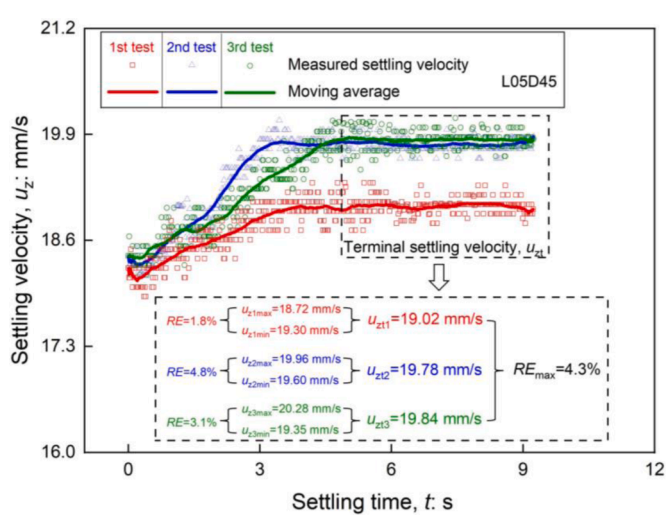

Fig. 2. Time-history of the measured settling velocity of a microplastic fiber. The length and diameter of the fiber are 5 mm and 0.45 mm, respectively. Measurements are taken (i.e., $t = 0$) when the fiber is 70 mm beneath the water surface. The relative error (*RE*) is calculated as $\frac{\text{maximum velocity} - \text{minimum velocity}}{\text{minimum velocity}} \times 100\%$.

further demonstrate that microplastic fibers indeed traverse laterally as a result of secondary motions.

These results are not surprising because microplastic fibers satisfy the criteria for the onset of secondary motions of a settling particle. More specifically, a settling cylindrical particle with an aspect ratio (i.e., the ratio of length to diameter) that is greater than 1.7 may exhibit secondary motions (Christiansen and Barker, 1965; Mando and Rosendahl, 2010). As such, the microplastic fibers, with aspect ratios from 5 to 34, used in this study were observed to exhibit secondary motions. As discussed, secondary motions are initiated by wakes behind a settling particle. Jayaweera and Mason (1965) reported that wakes appear as the Reynolds number becomes larger than 26 for a cylindrical particle. The Reynolds numbers of microplastic fibers used in this study range from 30 to 88. Furthermore, the Reynolds number of microplastic fibers that are settling in quiescent water can be up to 157 in the experiments reported by Khatmullina and Isachenko (2017). Taken together, it can be concluded that microplastic fibers are prone to secondary motions as they settle in water.

3.3. Settling orientation

The temporal evolutions of the settling orientation of all microplastic fibers tested in this study are provided in Section SM10 of the Supplementary Material. Since all tests exhibit a similar trend, only a typical test result (i.e., L05D65) is shown (Fig. 4).

It can be found that the orientation of a settling fiber changes during its acceleration and steady stages. It is evident that the settling motion of a given microplastic fiber is an orientation-dependent process. Moreover, the settling orientations of all microplastic fibers tested in this study appear to show a sinusoidal dependency with time (Fig. S12). As such, the relationship between the settling orientation and time can be expressed as follows:

$$\theta = A\sin(Bt + C) + D \tag{6}$$

where *A, B, C*, and *D* are constants that represent the amplitude, phase, phase shift, and amplitude shift, respectively. The sinusoid-dependent orientation of a settling slender body (e.g., needle, rod, and fiber) has also been reported by Toupoint et al. (2019). While we cannot observe a whole sine period for the fibers in this study due to our limited column height, it is still possible to deduce that the settling orientation of a microplastic fiber oscillates following a sinusoidal pattern.

It should be noted that, while the settling orientation of all microplastic fibers tested in this study exhibits a similar sinusoidal trend, the sinusoid-dependent orientations of each microplastic fiber has different constants (Eq. (6)). This is not surprising because the microplastic fibers used in different tests exhibit different settling velocities, and thus they have different total settling times.

Therefore, to quantify the temporal variation of the settling orientation, a characteristic time scale is required to enable a comparison of the settling times of the microplastic fibers used in different tests. More specifically, the instantaneous settling time (e.g., settling time shown in Figs. 2 and 4) from different tests needs to be normalized. The dimensionless settling time (t^*), which is calculated as the ratio of the instantaneous settling time (t) to the total settling time (T), i.e., $t^*=t/T$, is used as a characteristic time scale for all of the tested microplastic fibers. Therefore, as shown in Fig. 5, the expression of the sinusoid-dependent orientations for all tested microplastic fibers in this study can be obtained by using non-linear regression:

$$\theta = 3.8sin(4.5t* + 2.2) + 7.4 \tag{7}$$

While Eq. (7) can be used to predict the temporal variation of the settling orientation of a given microplastic fiber, the dimensionless settling time ($t^*=t/T$) in Eq. (7) must be known a priori. However, the total settling time (T), which is used to calculate t^*, cannot be obtained before conducting a test. Therefore, for time-resolved modeling of

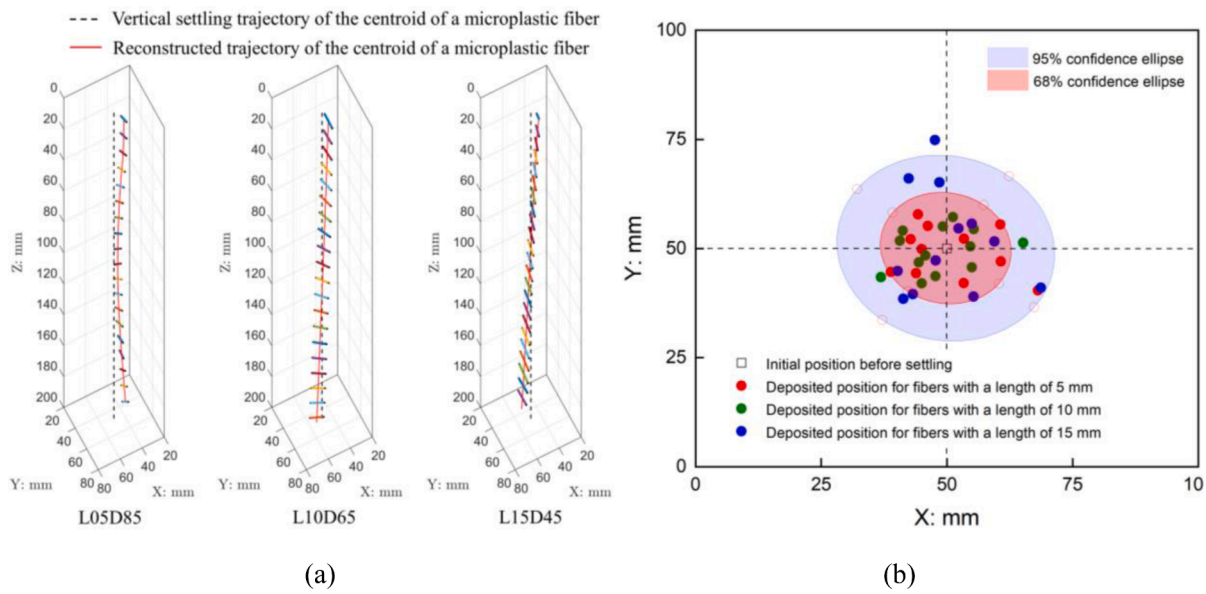

Fig. 3. Settling trajectory and final deposited position. (a) Reconstructed 3D trajectories of three microplastic fibers (test ID: L05D85, L10D65, and L15D55) used in this study. Measurements are taken (i.e., z= 0) when the fiber is 80 mm beneath the water surface. The time interval between each settling position of the microplastic fiber is 0.3 s; and (b) final deposited positions of all microplastic fibers tested in the experiments of this study.

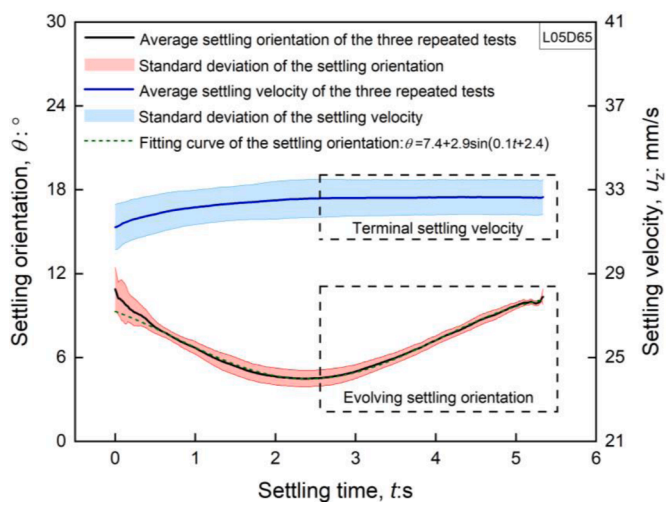

Fig. 4. Temporal evolution of the settling orientation of a microplastic fiber. The length and diameter of the microplastic fiber are 5 mm and 0.65 mm, respectively (test ID: L05D65).

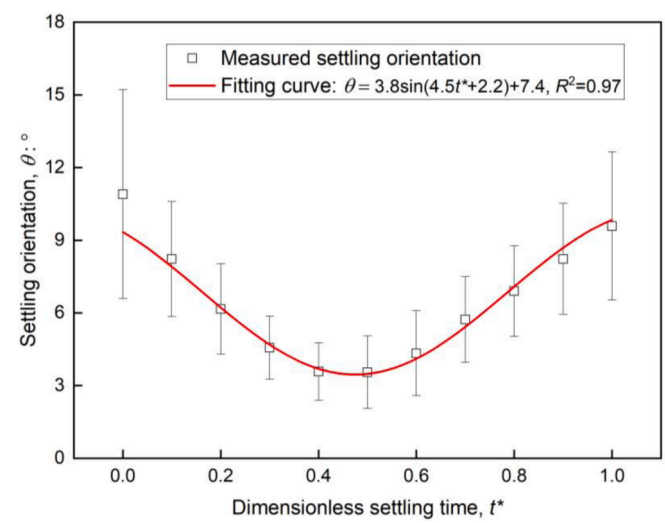

Fig. 5. Relationship between measured settling orientations and dimensionless settling time. The error bar means the standard deviation of the results of three repeated tests.

microplastic transport (e.g., Eq. (1)), it is not trivial to directly incorporate the predicted settling orientation (Eq. (7)) into the governing equations. To enhance the scalability of the prediction model of the settling orientation (Eq. (7)), the total settling time (T) should be obtainable based on measurable parameters (e.g., microplastic fiber dimension, density, volume, etc.).

Waldschlager and Schuttrumpf (2019) reported that the settling velocities of microplastics are linearly dependent on the dimensionless fiber diameter ($D^* = \sqrt[3]{LD^2(\rho_m/\rho_f - 1)g/\vartheta^2}$, where ϑ is the viscosity of the fluid). Similarly, a linearly-dependent relationship between the average settling velocities and dimensionless fiber diameters is observed in this study (Fig. 6a).

Moreover, the settling distances of all tested microplastic fibers is constant (Fig. 3a). Thus, it is reasonable to hypothesize that the total settling time of each microplastic fiber, which is the ratio of settling distance to the average settling velocity, is also dependent on the dimensionless fiber diameter. Fig. 6b shows the relationship between the total settling time and dimensionless fiber diameter. It can be observed that the total settling times exhibit a linearly-dependent relationship with the dimensionless fiber diameter:

$$T = -0.11\ D* + 11.01 \tag{8}$$

By combining Eq. (7) with Eq. (8), the prediction model of the settling orientations of a microplastic fiber can be recasted as:

$$\theta = 3.8\sin\left(\frac{4.5}{-0.22D^* + 11.01}t + 2.2\right) + 7.4 \tag{9}$$

The dimensionless fiber diameter ($D^* = \sqrt[3]{LD^2(\rho_m/\rho_f - 1)g/\vartheta^2}$) can be determined a priori since both the fiber (i.e., L, D, ρ_m) and fluid (i.e., ρ_f, ϑ) properties are measurable. As such, the settling orientation of a microplastic fiber can be estimated by using Eq. (9) at each time step for

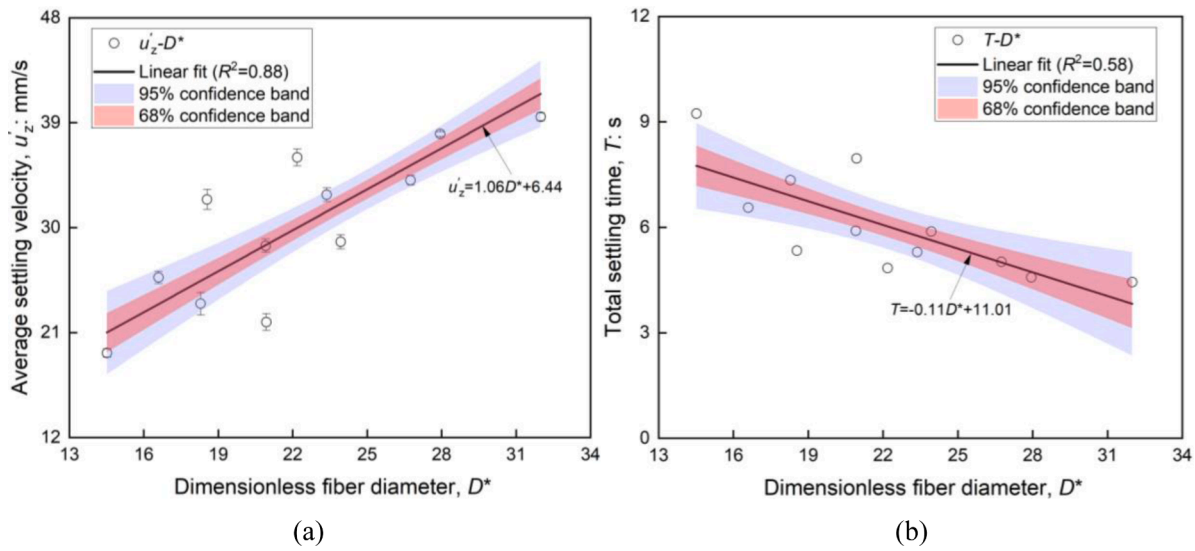

Fig. 6. Relationship between settling velocity, total settling time, and dimensionless fiber diameter. (a) Relationship between settling velocities and dimensionless fiber diameter. The average value of all measured velocities from each test is used. The error bars show the standard deviation of the results from the three repeated tests; and (b) relationship between the total settling time and dimensionless fiber diameter.

time-resolved modeling based on the Lagrangian particle-tracking method (e.g., Eq. (1)). To evaluate the developed model for predictions of the settling orientation of a given microplastic fiber (Eq. (9)), the calculated settling orientation (θ_{cal}) is compared with that measured (θ_{mea}) in Fig. 7. The average error (AE), which is calculated by using Eq. (10), can be used to statistically evaluate the performance of the proposed model (Eq. (9)):

$$AE = \frac{1}{n}\sum_{i=1}^{n}\left|(RE)_i\right| \times 100\% = \frac{1}{n}\sum_{i=1}^{n}\left|\frac{(\theta_{\mathrm{cal}})_i}{(\theta_{\mathrm{mea}})_i} - 1\right| \times 100\% \tag{10}$$

It can be found that the proposed model (Eq. (9)) reasonably predicts the instantaneous settling orientation with average errors that range from 7% to 53%. Also, it can be observed that the magnitudes of the settling orientations are from 3° to 15° with an average of about 6°. These orientations are not surprising because the extent of secondary motions (i.e., the magnitude of the settling orientation) is positively correlated to the extent of wake instability behind a settling microplastic fiber. Jayaweera and Mason (1965) reported that a wake behind a settling cylinder appears when the Reynolds number is larger than 26 and the extent of wake shedding increases with the Reynolds number. The Reynolds numbers of all the microplastic fibers used in this study are from 30 to 88. Thus, the magnitude of the settling orientations starts from 3° and covers a relatively small range (i.e., 3° ~ 15°). Toupoint et al. (2019) observed the settling orientation of about 7°for a cylinder with an aspect ratio (L/D) of 12 settling in quiescent water, which agrees with the range of the settling orientations (3° ~ 15°) and aspect ratios (5 ~ 34) of the microplastic fibers used in this study.

3.4. Drag coefficient

The temporal evolution of the drag coefficients of all microplastic fibers tested in this study are provided in Section SM11 of the Supplementary Material. It can be found that, throughout the entire settling

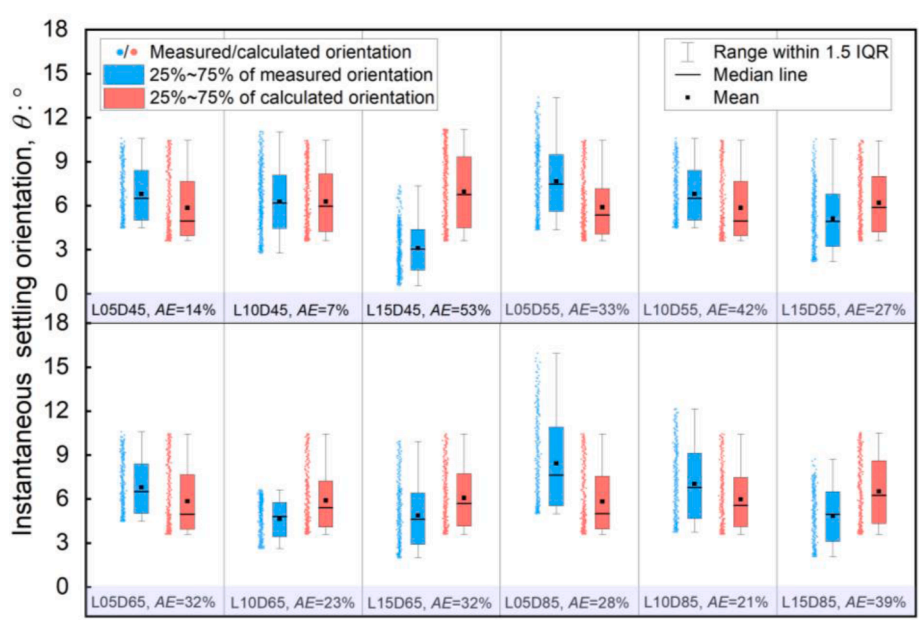

Fig. 7. Comparison between calculated and measured settling orientations of microplastic fibers.

process (i.e., both acceleration and steady stages), the drag coefficient is strongly influenced by the time-varying orientation of a microplastic fiber. More specifically, there is a positive correlation between the drag coefficient and settling orientation. This further demonstrates the impact of secondary motions on the hydrodynamics of a settling microplastic fiber.

Fig. 8 compares the drag coefficients calculated by using existing models ($C_{D,cal}$) with the ones measured in this study ($C_{D,mea}$). It should be noted that the drag coefficients shown herein are time-average ones from each experiment. Also, the average errors, which are calculated by substituting the settling orientations in Eq. (10) with the drag coefficients, are shown to statistically evaluate the performance of existing drag models. Moreover, all models evaluated herein were proposed for the characterization of the settling motion of a single particle in quiescent water.

It can be observed that the drag models proposed by Holzer and Sommerfeld (2008), Song et al. (2017), and Zhang and Choi (2022) show relatively low average errors (i.e., AE=33%, 34%, and 36%, respectively) for the predictions of the orientation-dependent drag coefficients of microplastic fibers. These results are not surprising because the models proposed by Holzer and Sommerfeld (2008) and Song et al. (2017) adopt crosswise sphericity, which is an orientation-dependent shape factor, to characterize the influences of settling orientations on drag coefficients. In contrast, the model proposed by Zhang and Choi (2022) adopts the Aschenbrenner shape factor to characterize the unique shape of microplastic fibers. The prediction errors of the models proposed by Holzer and Sommerfeld (2008) and Song et al. (2017) mainly stem from the use of less suitable shape factors to describe the morphology of fibers (i.e., the sphericity and crosswise sphericity). The prediction error of the model proposed by Zhang and Choi (2022) mainly stems from neglecting the orientation dependency of the settling process of microplastic fibers because the Aschenbrenner shape factor is independent of the settling orientation.

However, the drag models proposed by Khatmullina and Isachenko (2017), Waldschlager and Schuttrumpf (2019), and Dioguardi et al. (2018) exhibit relatively large average errors (i.e., AE=55%, 62%, and 104%, respectively). The large errors are because the three models do not consider the effects of settling orientations on the drag coefficients. Moreover, Khatmullina and Isachenko (2017) did not use a shape factor to account for the morphology of microplastic fibers, and Waldschlager and Schuttrumpf (2019) and Dioguardi et al. (2018) used the unsuitable shape factors (i.e., the Corey shape factor and sphericity) for characterizing the morphology of microplastic fibers (Zhang and Choi, 2022).

Taken together, to improve the predictions of the orientation-dependent drag coefficients of microplastic fibers, both the crosswise sphericity and Aschenbrenner shape factor need to be considered. This is because the crosswise sphericity can account for the settling orientation (Holzer and Sommerfeld, 2008; Song et al., 2017) while the Aschenbrenner shape factor can characterize the unique morphology of microplastic fibers (Zhang and Choi, 2022).

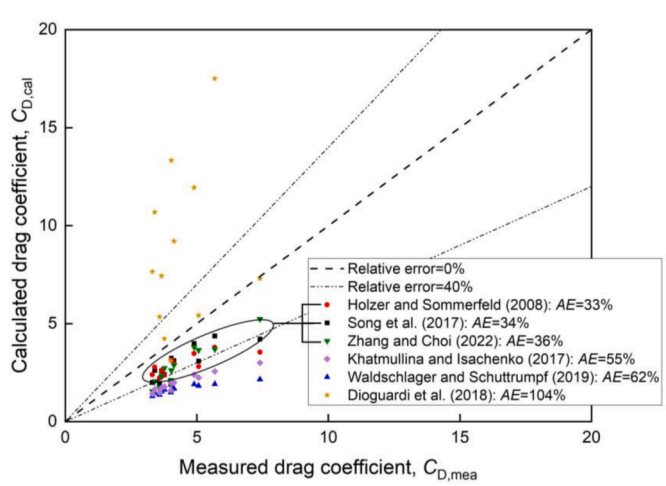

Fig. 8. Comparison of the calculated and measured drag coefficients of microplastic fibers for different drag models with the data set from this study.

3.5. New orientation-dependent drag model

To develop and evaluate a new drag model, the data sets, which include information on the drag coefficient, settling velocity, settling orientation, and physical properties (e.g., dimension, density, mass) of the microplastic fibers are required. Under circumstances where data is limited, researchers in the fields of geological sciences (Dioguardi et al., 2018) and industrial processing (Song et al., 2017) have resorted to using the same data set to develop and evaluate their proposed models. In fact, even well-established drag models in the literature for microplastic fibers were developed and evaluated in the same manner (Khatmullina and Isachenko, 2017). However, such an approach may not be ideal and subject to probity.

Due to the lack of data on the settling orientation of microplastic fibers in the literature and the need to address the shortcomings of using the same data set for model development and evaluation, we adopt a test/training split method (Singh et al., 2021). More specifically, we adopt a 50/50 split ratio. This means that 50% of the experimental data set produced in this study (i.e., L05D45, L05D55, L10D55, L10D65, L15D65, and L15D85) is used to develop the new model, and the unused 50% of the data set (i.e., L05D65, L05D85, L10D45, L10D85, L15D45, and L15D55) is used to evaluate the model.

Based on the 50% of the data set from the experiments conducted in this study, the crosswise sphericity is incorporated into the drag model proposed by Zhang and Choi (2022) using nonlinear regression. Consequently, the new orientation-dependent model is expressed as follows:

$$C_D = \frac{41.28 ASF^{0.49} S_c^{0.82}}{Re^{0.7}} \tag{11}$$

where ASF is the Aschenbrenner shape factor (ASF=L/D), and S_c is the crosswise sphericity ($S_c = \sqrt{6\pi V_m}/4DL\cos\theta$). Note that the microplastic fibers are herein assumed to be straight and non-deformable cylinders with circular cross-sections (Khatmullina and Isachenko, 2017). The Reynolds number (Re) adopted is the same expression as the one used by Zhang and Choi (2022), i.e., $Re = u_z\sqrt{4LD/\pi\vartheta^2}$.

Based on the unused 50% data set produced in this study, Fig. 9 shows a comparison of the performance between the measured drag coefficients and the ones calculated using the proposed model (Eq. (11)).

It can be observed that Eq. (11) can predict the orientation-dependent drag coefficients of microplastic fibers with relatively low average errors (i.e., AE=10.3%). Although the prediction errors for the microplastic fibers range from 1.5% (L15D45) to 21.3% (L10D85), the maximum prediction error (AE=21.3%) is still lower than the ones predicted using existing drag models (i.e., AE from 33% to 104% shown in Fig. 8). The predictions errors of L10D85 (i.e., AE=21.3%) and L05D85 (i.e., AE=19.6%) may be attributed to the method of preparation of the microplastic fibers adopted in this study. The microplastic fibers were cut from strands of polyester ropes so that the incised ends of some microplastic fibers are non-circular in cross-section (cf. the microscope images of L05D85 and L10D85 shown in Fig.S1). However, the cylinder with circular cross-section is a required assumption for calculations of the Aschenbrenner shape factor and crosswise sphericity. Thus, the microplastic fibers with non-circular ends exhibit slightly larger prediction errors (i.e., AE=21.3% for L10D85 and AE=19.6% for L05D85) compared with other fibers with more circular ends (i.e., $AE\leq$15.0% for L05D65, L10D45, L15D45, and L15D55).

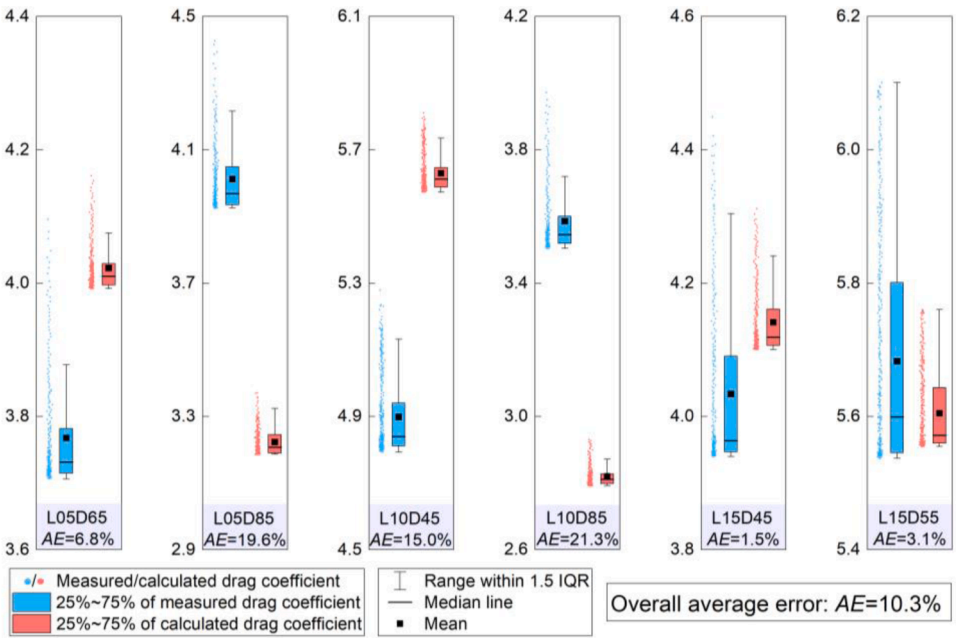

Fig. 9. Comparison of the measured and calculated drag coefficients of microplastic fibers for the proposed drag model (Eq. (11)) with the data set unused to develop Eq. (11).

4. Discussions

4.1. Applicability of experimental results

The diameters of the microplastic fibers used in the experiments of this study (i.e., 0.45 mm ~ 0.85 mm) are commonly used in similar settling experiments (Khatmullina and Isachenko, 2017; Waldschlager and Schuttrumpf, 2019). However, it is acknowledged that they may be larger than the ones detected in laundry effluent, which have diameters that are in the order of tens of μm (Hernandez et al., 2017; Napper and Thompson, 2016). Notwithstanding, microplastic fibers can be released from a multitude of other sources besides laundry effluent. These other sources produce fibers that are larger than those from laundry effluent. For instance, fishery activities are a significant source of microplastic fibers (Xue et al., 2020) and can generate fibers larger than 2 mm in diameter (Chen et al., 2018; Tan et al., 2020), which is larger than the fibers detected in laundry effluent (Wang et al., 2019). As such, the large microplastic fibers (0.45 mm ~ 0.85 mm) used in the experiments of this study also have relevance to those detected in natural aquatic environments.

The orientation-dependent drag model (Eq. (11)) was developed by using microplastic fibers with diameters ranging from 0.45 mm to 0.85 mm. Therefore, the applicability of Eq. (11) for modelling the secondary motions of fibers with smaller diameters needs to be evaluated. Fig. 10 shows the relationship between the maximum settling orientation of the microplastic fibers tested in this study and their corresponding Froude numbers (i.e., $Fr = \sqrt{\rho_m/\rho_w}\sqrt{D/L}$, which is a key parameter for the characterization of secondary motions (Chow and Adams, 2011). The maximum settling orientation (θ_{max}) can be used as a parameter to describe the extent of secondary motions (Will et al., 2021). It can be observed that there is an approximately linear relationship between the maximum settling orientation and Froude number:

$$\theta_{max} = 25.1Fr + 1.7 \tag{12}$$

Because the densities of water (ρ_w) and microplastic fibers (ρ_m) are constant variables, the Froude numbers of the settling microplastic fibers are dependent on their size (i.e., described using D and L). Consequently, the extent of secondary motions experienced is mainly dependent on the fiber size.

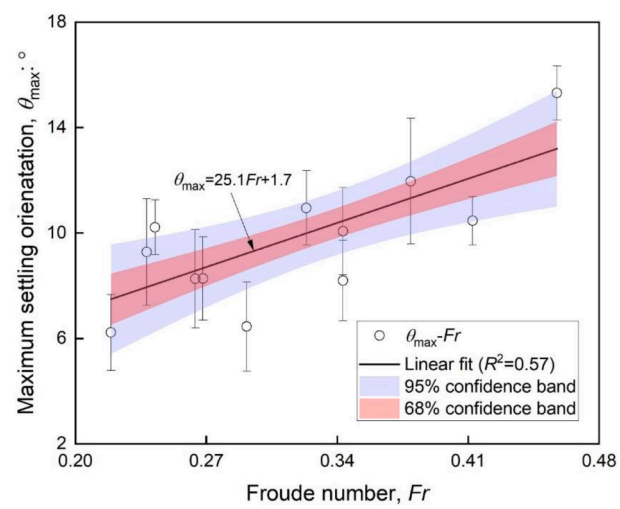

Fig. 10. Relationship between the maximum settling orientations and the Froude numbers of microplastic fibers. The error bars represent the standard deviation of the results of three repeated tests.

Fig. 11 shows the estimated maximum settling orientations for microplastic fibers with different sizes (i.e., described using the aspect ratio, L/D) and densities using Eq. (12).

A negative correlation between the maximum settling orientation and the aspect ratio can be observed. Also, it can be seen that, although the diameter of some microplastic fibers detected in the field (e.g., WWTP and laundry effluent) is in the order of tens μm (i.e., smaller than the ones used in this study), the fibers in the field exhibit larger aspect ratios (i.e., 46~655) than the ones used in this study (i.e., 5~34). As such, the maximum settling orientation detected in the field is smaller (e.g., less than 6° for microplastic fibers detected from WWTP and less than 4° for microplastic fibers detected from laundry effluent) than the ones observed in this study (i.e., less than 15°). This indicates that the secondary motions of microplastic fibers detected in the WWTP (Edo et al., 2020) and laundry effluent (Napper and Thomson, 2016) are weaker than the ones used in this study. The weaker secondary motions

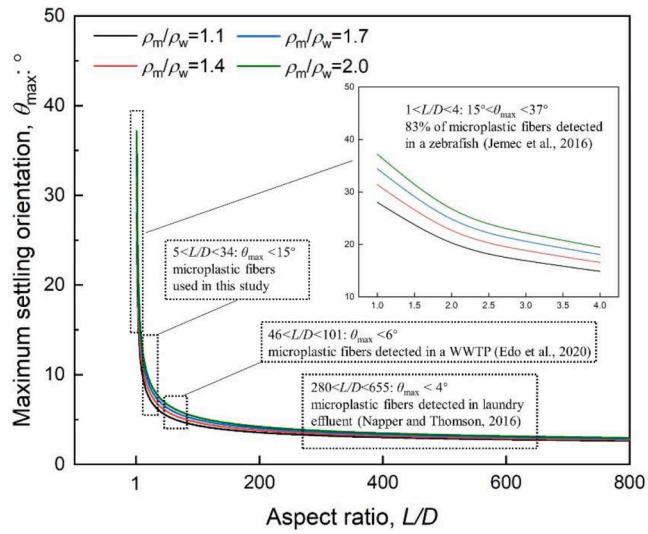

Fig. 11. Estimated maximum settling orientations of microplastic fibers with different aspect ratios and densities. The fiber densities, which are shown in the legend, are commonly found in natural aquatic environments (Chubarenko et al. 2016). The aspect ratios of microplastics detected in laundry effluent (Napper and Thomson, 2016), waste water treatment plant (WWTP) effluent and sludge (Edo et al., 2020), and zooplankton *crustacean daphnia* (Jemec et al. 2016), are shown. The inset shows a detailed view of the estimated maximum settling orientation of microplastic fibers with aspect ratios ranging from 1 to 4.

of microplastic fibers detected in WWTP and laundry effluent and the fibers used in this study (*Re* ranging from 30 to 88) belong to the laminar wake regime (i.e., $Re < 160$) as proposed by Bai and Alam (2018). Furthermore, Bai and Alam (2018) demonstrated that the drag coefficients (C_D) for all cylinders settling in the laminar wake regime exponentially decrease with an increase of Re, which is in agreement with the proposed drag model (i.e., $C_D \propto Re^{-0.7}$ in Eq. (11)). Evidently, the proposed model (Eq. (11)) can be used to characterize the secondary motions of microplastic fibers with aspect ratios larger than five.

The microplastic fibers detected in the food chain (Jemec et al., 2016) generally exhibit aspect ratios of less than four, which is smaller than the ones used in this study (i.e., 5~34). Consequently, the maximum settling orientation of the microplastic fibers detected in the food chain is larger (i.e., 15° ~ 37°) than the ones observed in this study (i.e., less than 15°). Since there is a positive correlation between the maximum settling orientation and the extent of secondary motions (Will et al., 2021), the microplastic fibers with aspect ratios of less than four will exhibit stronger secondary motions than the ones used in this study. As a result, the stronger secondary motions of fibers detected in the food chain may belong to the nonlaminar wake regime (Bai and Alam, 2018), where C_D increases with *Re*. Evidently, the proposed model (Eq. (11)), which was developed based on a laminar wake regime (i.e., C_D decreases with *Re*), may be less suitable for the characterizations of secondary motions of microplastic fibers with aspect ratios of less than four. Consequently, more data sets on the settling orientations of microplastic fibers that cover a broader range of aspect ratios will help to improve the proposed drag model (Eq. (11)).

From an experimental perspective, there are two additional reasons why microplastic fibers with larger diameters (i.e., 0.45 mm ~ 0.85 mm) are favorable. First, conventional image acquisition systems (i.e., the camera and image processing algorithm) have limited capacity to detect microplastic fibers with diameters in the order of tens of μm. Second, existing methods for preparing microplastic fibers, such as cutting or cryogenically grinding synthetic threads, cannot be used to prepare microplastic fibers that are less than 0.5 mm in size (Mossotti et al., 2021).

Another idealization made in this study is the use of relatively stiff microplastic fibers. In the field, microplastic fibers may be flexible and can bend as they settle Bagaev et al., 2017). Thus, the proposed drag model (Eq. (11)) may be less suitable for the characterizations of the settling motions of flexible microplastic fibers. The relatively stiff microplastic fibers used in this study only exhibit a slight curvature during the settling process (cf. Figs. S1 and S7b). As such, the microplastic fibers used in this study can be assumed to be straight and non-deformable cylinders, which is the common assumption for describing the microplastic fibers from fishing lines (Khatmullina and Isachenko, 2017) and idea for using the modified Maxey-Riley equation (i.e., Eqs. (1) and ((2)), which was developed for rigid particles. Evidently, further investigation on the transport of flexible microplastic fibers is warranted.

4.2. *Implications for the transport of microplastic fibers in natural aquatic environments*

This study is on the transport of microplastic fibers in quiescent water. Based on the modified Maxey-Riley equation (Eq. (2)), the proposed drag model (Eq. (11)) can be used for making predictions of the transport of microplastic fibers in enclosed and semi-enclosed aquatic bodies (e.g., bay water). This is because enclosed and semi-enclosed aquatic bodies may be idealized as quiescent water conditions (Zazouli et al., 2022) with inactive water exchange and wave conditions (Chen et al., 2018).

However, non-quiescent water conditions with waves and currents (e.g., rivers and oceans) are more common aquatic environments (Bagaev et al., 2017). In fact, microplastic fibers will settle under much higher Reynolds numbers in non-quiescent water conditions compared with the Reynold numbers in quiescent water conditions. Higher Reynolds numbers mean that secondary motions are more significant due to the enhanced wake instabilities produced behind the settling particles (Mando and Rosendahl, 2010). Thus, the drag model (Eq. (11)), which was proposed based on quiescent water conditions is less suitable for non-quiescent water conditions. Furthermore, fibers settling at higher Reynolds numbers are prone to longer transport distances in the horizontal direction (i.e., more significant lateral motions). This is caused by the enhanced turbulence generated by waves (Kerpen et al., 2020) or/and currents (Pohl et al., 2020). However, the effects of turbulence on secondary motions are not considered in the proposed drag model (Eq. (11)), nor the modified Maxey-Riley equation (Eq. (2)). Further investigation of the effects of turbulence and extended applications of the proposed drag model for more natural aquatic environments is warranted.

5. Conclusions

The effects of secondary motions on the settling behavior of microplastic fibers were experimentally investigated. Due to the presence of secondary motions, the settling motion of microplastic fibers is an orientation-dependent process that follows a sinusoidal pattern, which governs the drag coefficient of a settling microplastic fiber. A new drag model is proposed to describe the effects of secondary motions on drag coefficients. The proposed drag model has been demonstrated to more accurately predict the drag coefficients of microplastic fibers compared to existing models that do not consider secondary motions. Combined with the modified Maxey-Riley equation, the proposed drag model can be used in future modeling to improve the prediction of microplastic fiber transport.

As the first step towards the realistic predictions of the transport of microplastic fibers in aquatic environments, only stiff microplastic fibers in quiescent water conditions were investigated in this study. However, to further improve the predictions of the transport of a wider range of microplastic fiber types, research is required to study the secondary motions of flexible microplastic fibers settling in non-quiescent water conditions.

Supplementary materials

Supplementary materials associated with this article can be found in the online version.

Declaration of Competing Interest

The authors declare that they have no known competing financial interests or personal relationships that could have appeared to influence the work reported in this paper.

Acknowledgment

This work was supported by the Research Grants Council of Hong Kong (General Research Fund Grants 16209717; 16210219; 27205320; AoE/E-603/18).

Supplementary materials

Supplementary material associated with this article can be found, in the online version, at doi:10.1016/j.watres.2022.118476.

References

Bagaev, A., Mizyuk, A., Khatmullina, L., Isachenko, I., Chubarenko, I., 2017. Anthropogenic fibres in the Baltic Sea water column: field data, laboratory and numerical testing of their motion. Sci. Total. Environ. 599-600, 560–571.
Bagheri, G., Bonadonna, C., 2016. On the drag of freely falling non-spherical particles. Powder Technol. 301, 526–544.
Bai, H., Alam, Md.M., 2018. Dependence of square cylinder wake on Reynolds number. Phys. Fluids 30, 015102.
Bessa, F., Barria, P., Neto, J.M., Frias, J.P.G.L., Otero, V., Sobral, P., Marques, J.C., 2018. Occurrence of microplastics in commercial fish from a natural estuarine environment. Mar. Pollut. Bull. 128, 575–584.
Blettler, M.C.M., Abrial, E., Khan, F.R., Sivri, N., Espinola, L.A., 2018. Freshwater plastic pollution: Recognizing research biases and identifying knowledge gaps. Water Res. 143, 416–424.
Carranza, F., Zhang, Y., 2017. Study of drag and orientation of regular particles using stereo vision, Schlieren photography and digital image processing. Powder Technol. 311, 185–199.
Chen, G., Li, Y., Wang, J., 2021. Occurrence and ecological impact of microplastics in aquaculture ecosystems. Chemosphere 274, 129989.
Chen, M., Jin, M., Tao, P., Wang, Z., Xie, W., Yu, X., Wang, K., 2018. Assessment of microplastics derived from mariculture in Xiangshan Bay. China. Environ. Pollut. 242, 1146–1156.
Chow, A.C., Adams, E.E., 2011. Prediction of drag coefficient and secondary motion of free-falling rigid cylindrical particles with and without curvature at moderate Reynolds number. J. Hydraul. Eng. 137 (11), 1406–1414.
Chubarenko, I., Bagaev, A., Zobkov, M., Esiukova, E., 2016. On some physical and dynamical properties of microplastic particles in marine environment. Mar. Pollut. Bull. 108 (1-2), 105–112.
Christiansen, E.B., Barker, D.H., 1965. The effect of shape and density on the free settling of particles at high Reynolds numbers. AIChE J. 11 (1), 145–151.
Cowger, W., Gray, A.B., Guilinger, J.J., Fong, B., Waldschlager, K., 2021. Concentration depth profiles of microplastic particles in river flow and implications for surface sampling. Environ. Sci. Technol. 55 (9), 6032–6041.
DiBenedetto, M.H., Ouellette, N.T., Koseff, J.R., 2018. Transport of anisotropic particles under waves. J. Fluid Mech. 837, 320–340.
Dioguardi, F., Mele, D., Dellino, P., 2018. A new one-equation model of fluid drag for irregularly shaped particles valid over a wide range of reynolds number. J. Geophys. Res. Solid Earth 123 (1), 144–156.
Edo, C., Gonzalez-Pleiter, M., Leganes, F., Fernandez-Pinas, F., Rosal, R., 2020. Fate of microplastics in wastewater treatment plants and their environmental dispersion with effluent and sludge. Environ. Pollut. 259, 113837.
Gollin, D., Brevis, W., Bowman, E.T., Shepley, P., 2017. Performance of PIV and PTV for granular flow measurements. Granul. Matter. 19, 42.
Hernandez, E., Nowack, B., Mitrano, D.M., 2017. Polyester Textiles as a source of microplastics from households: a mechanistic study to understand microfiber release during washing. Environ. Sci. Tech. 51 (12), 7036–7046.
Holzer, A., Sommerfeld, M., 2008. New simple correlation formula for the drag coefficient of non-spherical particles. Powder Technol. 184 (3), 361–365.
Jayaweera, K.O.L.F., Mason, B.J., 1965. The behavior of freely falling cylinders and cones in a viscous fluid. J. Fluid Mech. 22, 709–720.
Jemec, A., Horvat, P., Kunej, U., Bele, M., Krzan, A., 2016. Uptake and effects of microplastic textile fibers on freshwater crustacean *Daphnia magna*. Environ. Pollut. 219, 201–209.
Kerpen, N.B., Schlurmann, T., Schendel, A., Gundlach, J., Marquard, D., Hupgen, M., 2020. Wave-induced distribution of microplastic in the surf zone. Front. Mar. Sci. 7, 590565.
Khatmullina, L., Isachenko, I., 2017. Settling velocity of microplastic particles of regular shapes. Mar. Pollut. Bull. 114 (2), 871–880.
Mando, M., Rosendahl, L., 2010. On the motion of non-spherical particles at high Reynolds number. Powder Technol. 202, 1–13.
Mossotti, R., Fontana, G.D., Anceschi, A., Gasparin, E., Battistini, T., 2021. Preparation and analysis of standards containing microfilaments/microplastic with fibre shape. Chemosphere 270, 129410.
Mrokowska, M.M., 2018. Stratification-induced reorientation of disk settling through ambient density transition. Sci. Rep. 8, 412.
Napper, I.E., Thompson, R.C., 2016. Release of synthetic microplastic plastic fibres from domestic washing machines: Effects of fabric type and washing conditions. Mar. Pollut. Bull. 112, 39–45.
Nguyen, T.H., Tang, F.H.M., Maggi, F., 2020. Sinking of microbial-associated microplastics in natural waters. PLoS ONE 15 (2), e0228209.
Piccardi, M., 2004. Background Subtraction Techniques: a Review, 4. IEEE, pp. 3099–3104.
Pohl, F., Eggenhuisen, J.T., Kane, I.A., Clare, M.A., 2020. Transport and burial of microplastics in deep-marine sediments by turbidity currents. Environ. Sci. Technol. 54 (7), 4180–4189.
Qureshi, M.H., Tien, W., Lin, Y.P., 2020. Performance comparison of particle tracking velocimetry (PTV) and particle image velocimetry (PIV) with long-exposure particle streaks. Meas. Sci. Technol. 32 (2), 024008.
Roy, N., Wijaya, K.P., Götz, T., Sundar, S., 2022. Transport of ellipsoidal microplastic particles in a 3D lid-driven cavity under size and aspect ratio variation. Appl. Math. Comput. 413, 126646.
Senathirajah, K., Attwood, S., Bhagwat, G., Carbery, M., Wilson, S., Palanisami, T., 2021. Estimation of the mass of microplastics ingested – a pivotal first step towards human health risk assessment. J. Hazard. Mater. 404, 124004.
Singh, V., Pencina, M., Einstein, A.J., Liang, J.X., Berman, D.S., Slomka, P., 2021. Impact of train/test sample regimen on performance estimate stability of machine learning in cardiovascular imaging. Sci. Rep. 11, 14490.
Song, X., Xu, Z., Li, G., Pang, Z., Zhu, Z., 2017. A new model for predicting drag coefficient and settling velocity of spherical and non-spherical particle in Newtonian fluid. Powder Technol. 321, 242–250.
Tan, F., Yang, H., Xu, X., Fang, Z., Xu, H., Shi, Q., Zhang, X., Wang, G., Lin, L., Zhou, S., Huang, L., Li, H., 2020. Microplastic pollution around remote uninhabited coral reefs of Nansha Islands, South China Sea. Sci. Total. Environ. 725, 138383.
Toupoint, C., Ern, P., Roig, V., 2019. Kinematics and wake of freely falling cylinders at moderate Reynolds numbers. J. Fluid Mech. 866, 82–111.
Waldschlager, K., Schuttrumpf, H., 2019. Effects of particle properties on the settling and rise velocities of microplastics in freshwater under laboratory conditions. Environ. Sci. Technol. 53 (4), 1958–1966.
Wang, T., Zou, X., Li, B., Yao, Y., Zang, Z., Li, Y., Yu, W., Wang, W., 2019. Preliminary study of the source apportionment and diversity of microplastics: Taking floating microplastics in the South China Sea as an example. Environ. Pollut. 245, 965–974.
Will, J.B., Mathai, V., Huisman, S.G., Lohse, D., Sun, C., Krug, D., 2021. Kinematics and dynamics of freely rising spheroids at high Reynolds numbers. J. Fluid Mech. 912.
Wu, L., Shang, Q., Sun, Y., Bai, X., 2019. A self-adaptive correction method for perspective distortions of image. Front. Comput. Sci. 13 (3), 588–598.
Xue, B., Zhang, L., Li, R., Wang, Y., Guo, J., Yu, K., Wang, S., 2020. Underestimated microplastic pollution derived from fishery activities and "hidden" in deep sediment. Environ. Sci. Technol. 54 (4), 2210–2217.
Yin, C., Rosendahl, L., Knudsen Kær, S., Sorensen, H., 2003. Modelling the motion of cylindrical particles in a nonuniform flow. Chem. Eng. Sci. 58 (15), 3489–3498.
Zastawny, M., Mallouppas, G., Zhao, F., van Wachem, B., 2012. Derivation of drag and lift force and torque coefficients for non-spherical particles in flows. Int. J. Multiph. Flow. 39, 227–239.
Zazouli, M., Nejati, H., Hashempour, Y., Dehbandi, R., Nam, V.T., Fakhri, Y., 2022. Occurrence of microplastics (MPs) in the gastrointestinal tract of fishes: a global systematic review and meta-analysis and meta-regression. Sci. Total. Environ. 815, 152743.
Zhang, J., Choi, C.E., 2022. Improved settling velocity for microplastic fibers: a new shape-dependent drag model. Environ. Sci. Technol. 56 (2), 962–973.
Zhao, S., Wang, T., Zhu, L., Xu, P., Wang, X., Gao, L., Li, D., 2019. Analysis of suspended microplastics in the Changjiang Estuary: implications for riverine plastic load to the ocean. Water Res. 161, 560–569.
Zobkov, M.B., Esiukova, E.E., Zyubin, A.Y., Samusev, I.G., 2019. Microplastic content variation in water column: the observations employing a novel sampling tool in stratified Baltic Sea. Mar. Pollut. Bull. 138, 193–205.